CrossMark
click for updates

Graphene processing using electron beam assisted metal deposition and masked chemical vapor deposition growth

Andrew Merrell[a] and Feng Liu
Department of Materials Science and Engineering, University of Utah, 122 S Central Campus Dr., Salt Lake City, Utah 84112

(Received 19 February 2016; accepted 28 June 2016; published 18 July 2016)

The fabrication of graphene devices can be challenging due to exposure to harsh chemicals and mechanical wear such as ultrasonication used for cleaning in photolithography and metal deposition. Common graphene processing methods often damage fragile graphene sheets and can ruin the device during fabrication. The authors report a facile method to overcome many of these challenges, which is specifically compatible with graphene grown by chemical vapor deposition (CVD). Using e-beam assisted metal deposition to deposit fine platinum features, electrodes can be deposited directly on graphene while still on the copper foil used as the catalyst during the CVD growth. The graphene and electrodes are then transferred to an insulating substrate, without further processing. This method preserves the graphene/metal interface from exposure to harsh chemicals used in traditional lithography methods, and avoids many of the conventional processing steps, which can cause unwanted doping, and damage or destroy the graphene. The authors observe an increase in Raman D-mode in the graphene under the Pt deposit, which suggests that the deposition method facilitates chemisorption by slightly abrading the surface of graphene surface during deposition. Using e-beam assisted electrode deposition in conjunction with masked CVD graphene growth on copper, the authors show the feasibility of fabricating complete graphene devices without subjecting the graphene to lithography, plasma etching, metal lift-off steps, or even shadow mask processing. © *2016 American Vacuum Society*. [http://dx.doi.org/10.1116/1.4958795]

I. INTRODUCTION

Graphene is a material with huge potential for nanoelectronics applications. It has been demonstrated as a prospective material to replace copper interconnects,[1] and can enhance performance of radiofrequency circuits,[2] flexible touch screens,[3] implantable medical sensors and monitors,[4,5] magnetic sensors,[6] and photodetectors,[7] all which require processing to pattern and contact the graphene with metal. Large, continuous graphene sheets can be grown successfully on copper foils[8] via chemical vapor deposition (CVD). Following CVD growth, the graphene can be transferred from the catalyst foil to insulating substrates for patterning and device fabrication. CVD growth has been demonstrated by many groups[9] and offers marked advantages as a graphene production method, despite challenges that arise in postprocessing. Improvements in processing methods are highly desirable, as exposure of graphene to various chemicals used for lithography can cause unwanted effects on the graphene,[10] and have detrimental impacts on the contact resistance.[11] Furthermore, many of the steps involved in traditional processing can lead to physical damage or destruction of the graphene sheet.

A. Traditional graphene patterning and processing methods

Photolithography (PL) and e-beam lithography (EBL) are the most common processing methods for CVD-grown graphene. The production of a graphene device from a large graphene sheet typically involves two rounds of lithography. One lithography process is implemented to pattern the graphene itself, and a second lithography process is used to pattern openings for electrodes, where metal can be deposited to contact the graphene. A typical patterning processes using PL includes the following steps: applying photoresist via spin coating, aligning a mask to the graphene, exposing to UV light, developing the photoresist in a strong base, etching exposed graphene using reactive plasma, and removing excess photoresist in an organic solvent. Each of the steps exposes the graphene to mechanical or chemical wear, which has unwanted effects on the graphene. Figure 1(a) shows an optical image of a graphene device after the first PL process and highlights the damage that often results from such processing. While the patterned graphene bar should have a clearly defined rectangular outline with patterned circles, the edges have peeled away from the substrate and resulted in undesirable wrinkling and tearing, which renders the device unusable.

Following the graphene patterning, the second PL process is carried out to deposit electrodes on the patterned graphene structure. A lift-off resist and photoresist are often applied in sequence, followed by soft baking, alignment with the photomask, exposure, developing, and finally, metal deposition by evaporation or sputtering. After the metal is deposited on the patterned graphene, the final step is to lift off the unwanted metal and photoresists from the substrate. Typically, this is done by placing the wafer in an ultrasonic acetone bath, which can completely destroy the graphene. Figure 1(b) shows a completed graphene inductor device that underwent the two PL processes (graphene patterning and metal

[a]Electronic mail: amerrell@eng.utah.edu

Redistribution subject to AVS license or copyright; see http://scitation.aip.org/termsconditions. IP: 155.98.6.186 On: Tue, 02 Aug 2016 22:40:18

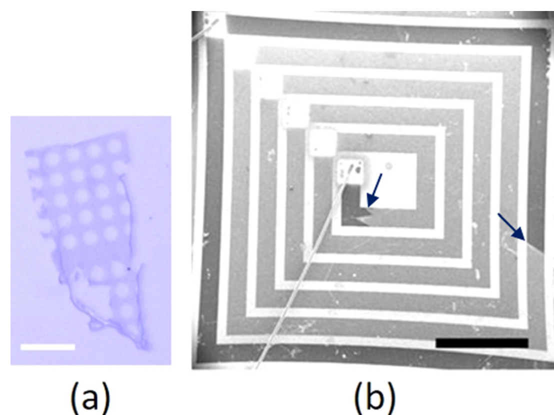

FIG. 1. (Color online) (a) Optical image of graphene showing damage after patterning by photolithography and O_2 plasma etching (scale bar 100 μm). (B) SEM image of graphene inductor device with square electrodes (Ti/Au) deposited on the outer corners. The center and outer electrodes are wire-bonded and grounded in the SEM chamber, so that the conductivity of the graphene is revealed by darkness contrast. Damage resulting from processing (indicated by arrows) shows the inductor loop is not conductive between the wire-bonded pads (scale bar 1 mm).

deposition). Wire bonds to the inner and outer electrodes were used to ground the device in the SEM chamber for inspection. Microscale scratches caused during processing define disconnected regions along the graphene path (extending from the wire bonds). Contrast between the dark gray graphene (connected to ground) and light gray (floating) indicate that the processing damage resulted in disconnection and device failure.

EBL is commonly used to pattern a resist-coated graphene sheet when the desired feature size is smaller than photolithography can achieve. Instead of UV light, EBL uses controlled rastering of an electron beam to selectively expose the resist and transfer the desired pattern. With a process flow analogous to PL, EBL processing can result in similar damage to the graphene. Imaging and exposing with the electron beam presents unique challenges, as well. For example, aligning the electrode mask to the graphene structure can be very difficult since the graphene is barely visible under a layer of resist, which is many times thicker than the graphene itself. This difficulty is further exacerbated by the fact that the graphene sits on an insulating substrate, which can lead to unwanted charging effects when imaging in the SEM. Lo-vac mode or integration mode are often necessary to properly focus the electron beam. Since the same beam is used for imaging and patterning the resist, one must also be extremely careful not to pattern unwanted areas while imaging.

Despite these challenges, several groups have succeeded in processing graphene using EBL and PL,[9,12] but have certainly invested extra time and care to keep the graphene intact throughout all the steps. Attempts have also been made to remedy these difficulties. For example, in patterning and processing of epitaxial graphene, Yang *et al.*[13] deposited an entire protective layer of Au or Pd/Au to prevent damage to the graphene during lithography, deposition, and lift-off steps. This was found to be effective in preventing damage to the graphene, though unintentional doping resulted after using aqua regia to remove the protective layer from the graphene. Other researchers have demonstrated the electrode deposition on graphene using a shadow mask,[14] which avoids the lithography steps associated with metal deposition, but presents additional challenges. For example, the shadow mask must come into very close contact with the graphene surface. This is experimentally challenging and is likely to result in scratches to the graphene surface. Another major difficulty is aligning the shadow mask with the underlying graphene structure. While alignment marks can aid in this process, the mostly opaque shadow mask severely limits the visibility of the underlying graphene.

B. Graphene processing using electron beam assisted metal deposition

In light of the difficulties associated with traditional processing methods, it is clear that a more effective processing method, which better accommodates the fragility of graphene, is highly desirable. Our new method implements localized e-beam assisted metal deposition, which we find is particularly compatible with CVD-grown graphene. The mechanism of deposition, described in detail elsewhere,[15,16] involves the decomposition of an organometallic gas on the graphene surface using a focused electron beam [or focused ion beam (FIB)] (FEI Helios Nanolab 650 and similar instruments have this capability). A platinum-containing precursor gas [$C_5H_4CH_3Pt(CH_3)_3$] was chosen for our experiments due to its widespread use and availability in our experimental facilities. Additionally, we note that platinum has relatively high carbon solubility,[17] partially filled D-electron orbitals, and a high work function, all which should facilitate low contact resistance with graphene. While the deposition of platinum electrodes on graphene using e-beam or FIB is not new,[18,19] the novelty of our work is in demonstrating that the electrode deposition can be performed on the graphene directly after CVD growth, while the graphene is still on the catalytic metal foil used in CVD. After the Pt is deposited, wet chemical transfer can be carried out to move the Pt/graphene to an insulating substrate. The basic process flow is illustrated schematically in Fig. 2. We demonstrate that the transfer of the Pt/graphene from copper to an insulating substrate can be carried out while keeping the platinum electrodes intact.

This method for contacting graphene circumvents the lithography and shadow mask processes, which often result in damage to the graphene. To circumvent lithography processing associated with graphene patterning (the first "round" of lithography described above), we show that the new deposition method can work in conjunction with masked graphene growth,[20] where graphene structures grow on prepatterned, Al_2O_3-masked copper foils in CVD. Using masked graphene growth in conjunction with e-beam assisted deposition, we demonstrate that complete graphene devices can be produced while completely avoiding lithographic, and shadow mask processing on graphene.

Redistribution subject to AVS license or copyright; see http://scitation.aip.org/termsconditions. IP: 155.98.6.186 On: Tue, 02 Aug 2016 22:40:18

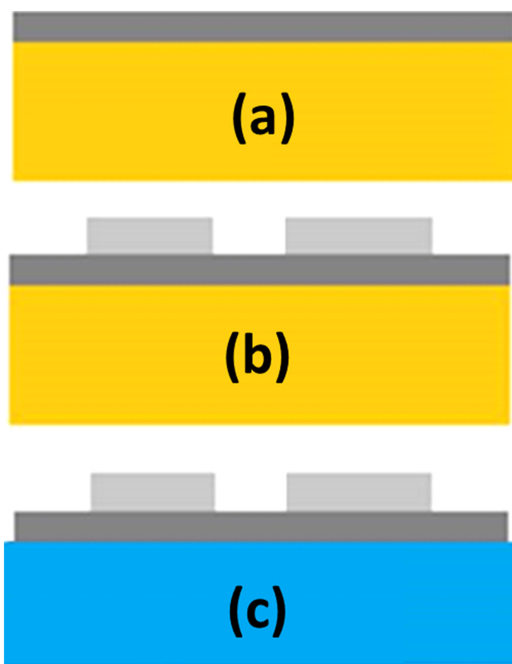

FIG. 2. (Color online) Process flow for new method of electrode deposition on CVD grown graphene. After the graphene is grown on the copper foil (a), the Pt electrodes are deposited on the surface of the graphene using the e-beam assisted deposition method (b). Afterward, the wet transfer is carried out, and the graphene with electrodes is transferred to an insulating substrate (c), avoiding e-beam lithography and photolithography.

It is likely that our newly proposed method will not possess the same parallel processing throughput as photolithography. However, the deposition process can still be automated by appropriately configuring the software on the deposition tool, and, at the least, our newly developed process is likely to be very helpful in laboratory- or prototype-scale device fabrication. This provides a useful supplement and/or a ready alternative to conventional methods. Our new e-beam assisted deposition method has several advantages over traditional graphene patterning methods. First, pristine contact between the electrode and graphene can be achieved, since the metal is deposited directly on the graphene immediately following CVD. The introduction of chemical contamination needed for traditional metal deposition techniques can be completely avoided. Even if additional contaminants are introduced after the Pt deposition, the interface should remain unaffected. This is also an advantage when compared to shadow-mask metal deposition, since alignment and close contact with the graphene surface is not necessary. Second, the deposition is easy to perform when the graphene is still on copper, as a conducting substrate eliminates charging effects that can often occur if the graphene is first transferred to an insulating substrate. Third, extremely small feature size is achievable by e-beam assisted metal deposition (better than photolithography). Fourth, when used in conjunction with masked CVD growth, complete devices can be produced with minimal graphene handling.

II. EXPERIMENT

In e-beam assisted metal deposition, the main parameter influencing the deposition time is the beam current. Figure 3 shows the relationship between e-beam current and deposition time for a fixed volume. It is important to note, however, that too high a beam current can cause sample etching or damage to the graphene. Even faster deposition times than observed in Fig. 3 can be achieved by implementing the FIB, though the high beam energy can quickly destroy the graphene. We chose a moderate e-beam current in order to achieve reasonable deposition times while still preserving the underlying graphene. Detailed analysis of the effect on graphene is presented in Sec. III.

After growing graphene films on Cu foils using atmospheric CVD (details provided in supplementary material),[40] we deposited Pt features on the graphene/copper stack using the e-beam assisted method. Though the FIB can easily destroy the graphene, the faster deposition rate is advantageous for depositing connections to the graphene electrodes that may later be contacted with testing probes. In other words, the FIB is not viable for contacting graphene, but is used as an aid in device fabrication. Following the Pt deposition, transfer was carried out using a traditional PMMA support technique (see supplementary material) to move the Pt/graphene from the copper to an insulating glass or SiO_2 substrate. We characterized the result by optical microscopy and Raman spectroscopy. Having demonstrated the successful transfer of platinum electrodes from the deposition on graphene/Cu to graphene/SiO_2, we used masked graphene growth to selectively grow graphene via CVD and successfully show that our proposed processing methods are capable of producing graphene devices with minimal graphene processing. Last, we performed electrical resistance measurements on the transferred graphene/Pt devices and report an order of magnitude estimation of the Pt/graphene contact resistance.

III. RESULTS

A. E-beam and FIB assisted deposition of Pt on graphene/Cu

The purpose of using both e-beam and FIB in the initial deposition was to (1) gain a general familiarity and understanding of the deposition parameters for the newly proposed

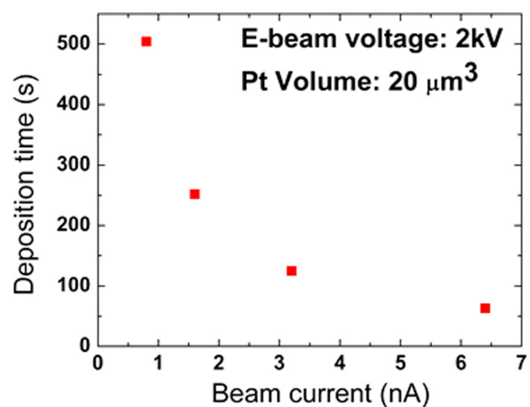

FIG. 3. (Color online) Empirically observed relationship between e-beam current and deposition time for a fixed 20 μm^3 volume of Pt at beam voltage 2 kV.

Redistribution subject to AVS license or copyright; see http://scitation.aip.org/termsconditions. IP: 155.98.6.186 On: Tue, 02 Aug 2016 22:40:18

methodology, (2) test the feasibility of transferring the Pt/graphene from the copper to an insulating substrate, and (3) observe any effects on the surrounding graphene caused by imaging by the electron beam or focused ion beam.

Figure 4 shows the SEM and optical images mirroring the process steps shown in Fig. 2. Figure 4(a) shows several Pt features deposited on the graphene/copper surface by e-beam and FIB. The small squares and vertical lines of 500 nm thickness were deposited by the e-beam at 2 kV and 3.2 nA, and the large squares (also 500 nm thick) were deposited by the FIB at 30 kV and 0.79 nA. These beam energies were chosen in order to allow for reasonable deposition times of 1–2 min. Several effects can be observed in the images in Fig. 4. First, the right vertical line shows some blurring which is due to small drift of the sample during the deposition. We found this can be mitigated by selecting a beam current and feature size to minimize the deposition time, and depositing the features one at a time, which helps ensure the sample has not drifted from the desired deposition area. Second, it can be seen in Fig. 4(c) that much of the area surrounding the deposition area has damaged graphene that is peeled or rolled back from the substrate. This highlights the damage caused by exposing the graphene to the high energy FIB. For this reason, the FIB was only used in subsequent experiments for depositing connecting wires to facilitate device testing, not as a method for contacting graphene. Third, we took care during the deposition to avoid exposing the area between the small squares to the FIB, though a short accidental exposure at the area indicated in Fig. 4(a) resulted in a damaged area after the transfer [see corresponding area in Fig. 4(c)]. This is most likely because the removal of the graphene exposes the Pt to the etching acid used in transfer. Though Pt should have a very low etching rate in CE-200,[21] the area of accidental exposure may result in some very slight Pt etching, and may also contain undissolved or partially dissolved copper. While this experiment demonstrates the successful transfer of Pt electrodes from the deposition on graphene/Cu to an insulating substrate, additional experiments were carried out to assess how the deposition and transfer affected the graphene.

B. Effect of Pt deposition and transfer on graphene

Figure 5 shows images from different stages of processing and demonstrates the successful deposition and transfer of Pt electrodes on CVD graphene. Figures 5(a) and 5(b) are the SEM and optical images of a 10 μm^2 platinum pad (thickness 200 nm) deposited on graphene/copper using the e-beam at voltage and current of 2 kV and 1.6 nA, respectively. These beam parameters were chosen as they still allowed for a reasonable deposition time, while likely minimizing any damage to the graphene during deposition. After transferring the Pt/graphene to an insulating glass substrate, the Pt electrode remains intact and unaffected as shown by optical image Fig. 5(c).

We performed a detailed Raman analysis on the as-transferred sample, and to assess the condition of the graphene under the Pt pad, we carried out a second identical Raman analysis after dissolving Pt pad in dilute aqua regia acid and exposing the underlying graphene. Figure 6(a) shows the optical image at 600× magnification of the as-transferred sample. From the “x” mark, individual representative spectra were taken before and after the Pt pad was dissolved, and results are shown in Fig. 6(b). The Raman images for characteristic graphene wavenumbers are also shown in Figs. 6(c)–6(h): (c) and (d) show the D- and G-mode images (1350–1580 cm^{-1}), (e) and (f) show the D-mode images (1310–1370 cm^{-1}), and (g) and (h) are the 2D-mode images (2635–2735 cm^{-1}). Two significant results obtained from the Raman analysis are discussed here.

First, the results show that the graphene underneath the platinum is not destroyed in the deposition or transfer process. In the Raman spectrum shown in Fig. 6(b) from the Pt pad, we observe the characteristic carbon G-mode at $\sim$1580 cm^{-1} (due to sp^2 carbon bonds) and a broad tail toward lower wavenumbers. The broad peak in this range is a signature of amorphous carbon[22] and is not due to the carbon in graphene which has much sharper peaks. The fact that this spectrum is not graphene is also confirmed by the lack of the signature 2D-mode that should be present for graphene at $\sim$2700 cm^{-1} [also evident from Fig. 6(g)]. The observance of amorphous carbon is expected, since it is well known that

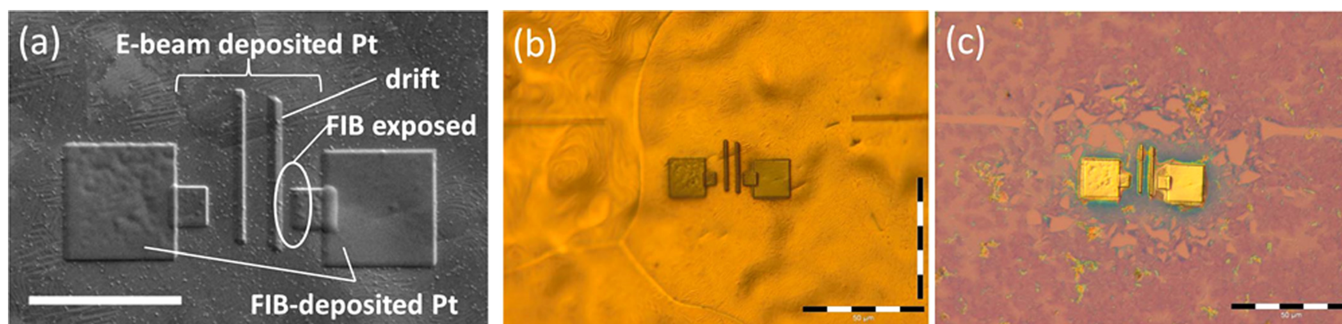

FIG. 4. (Color online) (a) SEM image of Pt deposition on graphene using both FIB and e-beam directly after CVD deposition. The Pt is deposited while the graphene is still on the copper catalyst used in CVD growth. Drift during the deposition can cause a smeared deposit to occur. Areas exposed to FIB result in damaged graphene which is visible after transferring to insulating substrate (scale bar 20 μm). (b) Corresponding optical image showing the Pt deposition on graphene/copper (scale bar 50 μm). (c) Optical image of Pt/graphene after the transfer to an insulating SiO_2 substrate is carried out. Pt contacts remain in intimate contact with the graphene. Above and below the Pt features, where the FIB was used to image or deposit Pt, damage to the graphene is observed (scale bar 50 μm).

Redistribution subject to AVS license or copyright; see http://scitation.aip.org/termsconditions. IP: 155.98.6.186 On: Tue, 02 Aug 2016 22:40:18

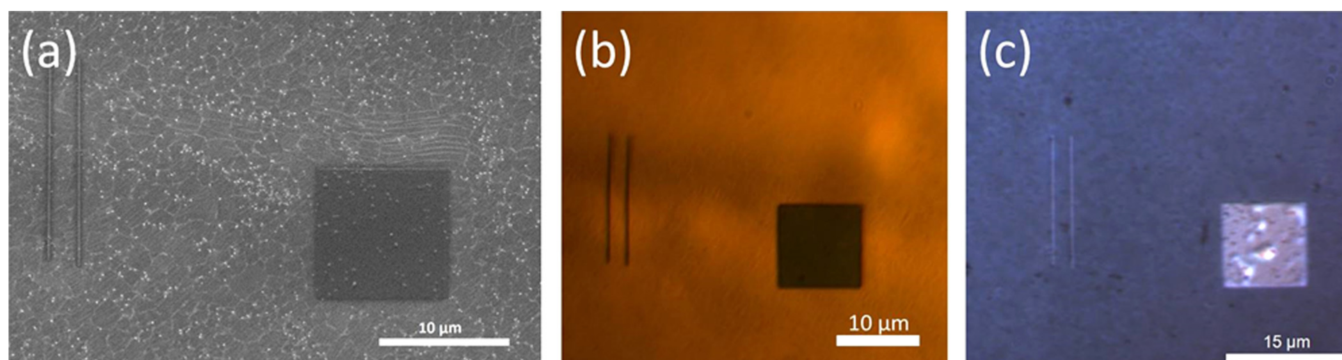

FIG. 5. (Color online) Process images of a 10 μm^2 Pt box deposited on graphene/copper and transferred to an insulating substrate. The Pt was deposited using e-beam assisted deposition with beam voltage and current of 2 kV and 1.6 nA, respectively. The SEM image directly after Pt deposition in (a), the optical image of Pt electrode on copper foil in (b), and the optical image after the graphene is transferred to an insulating substrate in (c) are shown.

Pt deposited by the e-beam assisted method contains unwanted remnants of the organometallic precursor,[23,24] which degrade electrical conductivity. This spectrum and corresponding Raman images are consistent, as we do not expect to detect graphene under the 200 nm layer of Pt. After the removal of Pt, however, we see in Fig. 6(b) that the sharpness of the peaks reappears, and the graphene 2D-peak is also visible. The Raman image in Figs. 6(g) and 6(h) shows that the 2D mode is absent when scanning on Pt, but after removal, the 2D-peak intensity blends uniformly with the surrounding graphene, indicating that the graphene still exists and is not obliterated during the deposition process. This confirms the effectiveness of our direct deposition and processing method, and shows that graphene remains intact during the deposition and through the transfer process.

The second and perhaps more significant result obtained by the Raman analysis is the emergence of the graphene D-peak after the Pt is removed. The peak is located at $\sim$1350 cm^{-1} and can be seen in Fig. 6(b) as well as the Raman images in Figs. 6(e) and 6(f). This peak in the graphene Raman spectrum is commonly referred to as the "defect peak" as it does not occur in perfectly crystalline graphene—it is the result of a two-phonon scattering process that occurs only at a boundary or defected area of the graphene.[25] We note that this peak has negligible intensity in the bulk graphene sheet (i.e., areas where Pt was not deposited). This is evidenced by the representative spectrum shown in Fig. 6(b) of the surrounding graphene as well as other Raman characterization performed on the bulk graphene, which is shown in supplementary material 1. The emergence of the D-mode, which appears in the graphene underneath the Pt, is evidence that the e-beam assisted deposition facilitates Pt chemisorption, as opposed to physisorption. The difference is an important distinction in the selection of a low contact resistance metal for graphene. Physisorbed metals indicate weak bonding to the graphene and should result in higher contact resistance than the predicted chemisorbed metals such as Co, Ni, Pd, and Ti.[26] Leong *et al.*[27] studied the effects of annealing various metal/graphene contacts and observed a similar increase in D-mode intensity of graphene after annealing nickel/graphene contacts. This was attributed to the partial absorption of carbon into the nickel contact during annealing. After dissolving the nickel contacts from graphene, Leong *et al.* showed that the D-mode was more prevalent due to defects in graphene caused by partial absorption of carbon into the Ni contact, facilitating bonding

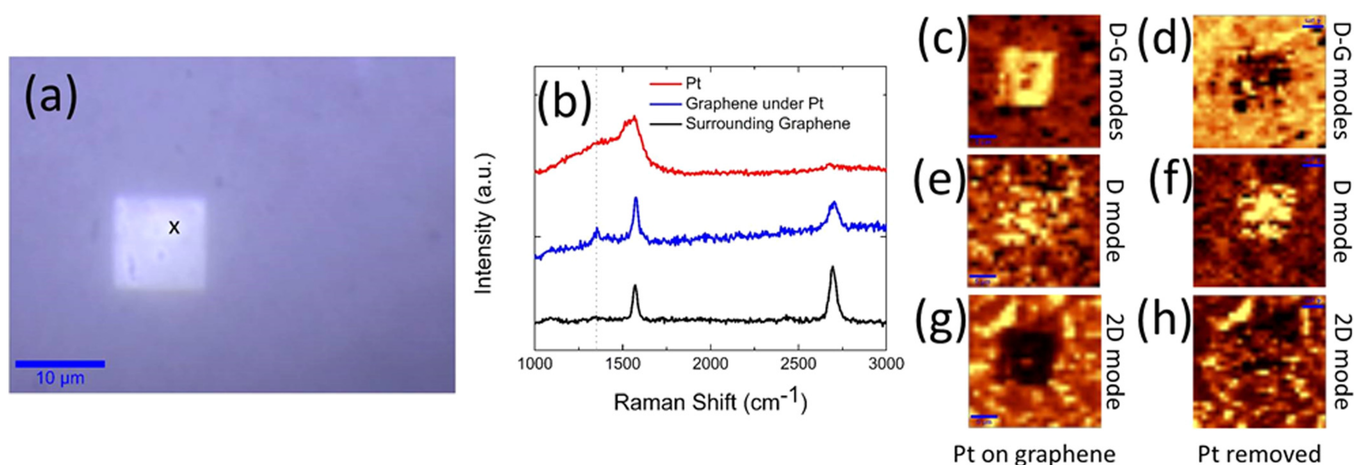

FIG. 6. (Color online) (a) Optical image of Pt/graphene transferred to glass substrate. (b) Representative Raman spectra taken from the point marked with an *x*. (c)–(h) Raman images of Pt on graphene before and after Pt pad is removed by diluted aqua regia. D-G modes (1350–1580 cm^{-1}) are shown in (c) and (d), D-mode (1310–1370 cm^{-1}) is shown in (e) and (f), and 2D mode (2635–2735 cm^{-1}) is shown in (g) and (h).

Redistribution subject to AVS license or copyright; see http://scitation.aip.org/termsconditions. IP: 155.98.6.186 On: Tue, 02 Aug 2016 22:40:18

and low contact resistance. Absorbed areas were removed with the nickel leaving behind defected graphene as evidence that strong bonding had occurred. In Leong's work, this mechanism was used to explain a very low contact resistance with graphene/nickel. We attribute the observed increase in the D-mode intensity to two similar mechanisms that are likely the result of the e-beam assisted deposition. First, local hydrogen species released from the cracked precursor gas can partially etch the graphene at the deposition site. This effectively roughens (abrades) the graphene surface by opening dangling bonds that can facilitate chemisorption and enhanced bonding between graphene and Pt. This etching effect has also been observed by others.[28] Second, localized heating at the deposition site may further facilitate carbon-platinum bonding. While several publications report that in theory, Pt should physisorb on graphene, the experimental results in the literature are commonly inconsistent. For example, while Ti is predicted to be chemisorbed on graphene, Nagashio *et al*. reported extremely large contact resistance for Ti/graphene when using RF sputtering.[29] For copper which should be physisorbed, Smith *et al*. showed that contact resistance with graphene can be significantly reduced by contact patterning and annealing.[30] The disparity between experimental findings and theoretical predictions suggests that the experimental factors such as the deposition method, and processing parameters such as annealing and contact patterning, may play a more important role than the metal choice itself. This has also been the conclusion of other research regarding graphene/metal contact resistance.[11] Therefore, the increase in the D-mode intensity suggests that our newly proposed method of contacting graphene may provide a method for effectively contacting graphene not only with Pt, but with other metals as well, since nearly all metals can be fabricated into a precursor gas compatible with e-beam assisted deposition.[31]

C. Al_2O_3 masked graphene growth with e-beam assisted Pt deposition

Thus far, we have discussed a method for depositing metal on CVD-grown graphene. Our proposed method can avoid excess handling and common damage that often results from conventional metal deposition techniques such as lithography or shadow mask processing. However, CVD graphene is produced in large-area sheets that must be patterned into device structures prior to metal deposition. Therefore, unless the graphene sheet can also avoid lithography associated with graphene patterning, our method does not provide much advantage. For this reason, we demonstrate the compatibility of e-beam assisted deposition with Al_2O_3 masked graphene growth. Masked graphene growth is a method by which prepatterned graphene structures can be grown in CVD, thus avoid postprocessing. The method is accomplished by lithographically patterning the copper catalyst foil prior to the CVD growth, and depositing a thin patterned mask of Al_2O_3, which serves as a barrier to graphene growth during CVD. Other groups have used e-beam lithography to pattern and mask copper foils, and have observed excellent resolution (~5 nm) in CVD-grown graphene structures.[20]

A patterned structure produced by masked graphene growth is shown in Fig. 7(a), where the darker contrast is a 100 μm wide graphene bar, and the lighter contrast is the Al_2O_3 masked copper foil. (Experimental methods for the masked growth process are described in supplementary material). After the graphene was grown on the masked copper surface, Pt electrodes were deposited on the graphene using the e-beam assisted deposition method (the deposition parameters were held at 2 kV and 1.6 nA). The FIB was used to deposit Pt wires connecting to the graphene/Pt electrodes that could later be contacted with silver paste to allow for two-probe electrical testing. Figure 7(b) shows the optical image of the Pt electrodes after e-beam assisted deposition, and Fig. 7(c) shows the final device after transferring to an insulating SiO_2 substrate. The final device has a structure similar to field effect transistors, or a transfer length method (TLM) device, used measure contact resistance, thus demonstrating the feasibility of using masked CVD growth with e-beam assisted deposition to create complete graphene devices.

Two artifacts can be noted from this device. First, the ~100 μm wide device shown in Fig. 7 is quite large for the

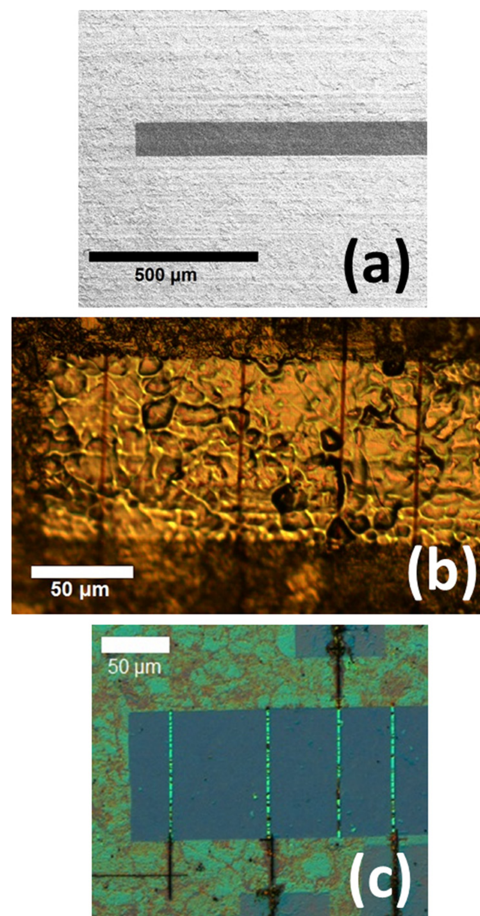

FIG. 7. (Color online) (a) SEM image of selectively grown graphene on copper foil. Darker contrast is graphene, and lighter contrast is Al_2O_3-masked copper. (b) Optical image of graphene bar on copper showing Pt electrodes deposited directly on selectively grown graphene. (c) Optical image of graphene and deposited Pt electrodes after transfer to insulating SiO_2 substrate.

Redistribution subject to AVS license or copyright; see http://scitation.aip.org/termsconditions. IP: 155.98.6.186 On: Tue, 02 Aug 2016 22:40:18

scale of nanoelectronics and graphene devices. Small wrinkles in the electrodes of the final device can be seen, and are attributed to the surface roughness of the copper foil. While even these large electrodes are still connected, we expect that a smoother copper surface, as well as a reduction in feature size will remove such defects, and the device shown here helps demonstrate the upper size limits of this technique. The second artifact observed in this device was evidenced by the FIB-deposited connecting wires shown in Fig. 7(c). The high energy of the FIB caused partial etching of the Al_2O_3 mask and resulted in an imprecise deposition. It was clear when depositing the Pt in these areas, that the surface roughness on the Al_2O_3 masked copper was greater than the thickness of the deposited electrodes, making it difficult to ensure that the thin Pt wires were continuously connected. These problems could be easily remedied by either using a different copper foil with a smoother finish, or employing a chemical/mechanical polishing method to smooth the copper surface prior to Al_2O_3 patterning, which is routinely done.[32] To remedy the unreliable FIB-deposited Pt connecting wires in this particular device, the wires were redeposited after transfer using e-beam assisted method with deposition parameters of 2 kV and 1.6 nA.

D. Estimation of contact resistance

To test the device, small spot of colloidal silver paste was deposited atop the Pt connecting wire using a micromanipulator under a microscope. We measured the two-probe resistance between adjacent electrodes by taking an I-V curve and sweeping the voltage from −1 to 1 V in steps of 0.01 V. An order of magnitude estimate of the contact resistance was taken based on the following model:

$$R_{Tot} = R_G + R_W + R_{Ag/Pt} + 2R_{CR},$$

where R_{Tot} is the total measured resistance, R_G is the resistance of the graphene, R_W is the resistance of the Pt wire, $R_{Ag/Pt}$ is the contact resistance of the silver paste with platinum wires, and R_{CR} is the platinum/graphene contact resistance. Assuming negligible resistance caused by the contact probes, we found that the Pt/graphene resistivity is on the order of $10^9\ \Omega\ \mu m$ (details of calculation given in supplementary material).

In various publications on graphene/metal contact resistance, reported values often vary by orders of magnitude, even for the same metal, and there is a lack of experimental measurements for Pt/graphene contact resistance in existing literature. Robinson *et al.*[11] reported contact resistivity for Pt/graphene in the range of 10–50 $\Omega\ \mu m^2$, and other researchers have used Pt only for theoretical studies,[26,33] or as a middle or capping layer for graphene contacted by another metal.[34] While Robinson's values are much lower than our estimate, order of magnitude differences in experimental findings are common. For example, Ti is commonly used to contact graphene, and the reported values range from $\sim 10^2$ (Ref. 35) to $\sim 10^9\ \Omega\ \mu m$.[29] This shows that our value, while high, is not unreasonable.

To suggest areas for future improvement of beam-assisted metal deposition, we outline three likely reasons for the high estimated contact resistance. First, the microstructure of Pt deposited by the e-beam assisted method is known to contain domains of amorphous carbon[36] as discussed and observed in the Raman analysis above. This may play a significant role in increasing the contact resistance since it decreases the number of Pt domains that contact the graphene. Amorphous carbon contamination in Pt deposits is a common problem with e-beam and FIB assisted Pt deposition, and methods for purification and carbon reduction have been studied by several groups.[18,23,36,37] Some of the methods used to purify Pt include annealing and laser treatment, and are likely compatible with Pt-contacted graphene. (We note that amorphous carbon contamination is typically rich in sp^3 bonds[38] and is thus easily distinguishable using Raman spectroscopy.[39]) Alternate Pt precursor gases which have been studied by others[18] may also significantly reduce such carbon domains and greatly reduce the contact resistance. Second, an underestimate of the contact resistance between the colloidal silver paste and Pt wire may account for an over-estimate of the Pt/graphene contact resistance reported here. Third, the graphene grown in our CVD system contained SiO_2 contamination [shown by the white dots in Fig. 5(a)] which naturally leads to higher contact resistance as it both lessens the contact interface area and degrades the electrical mobility.

IV. SUMMARY AND CONCLUSIONS

We have demonstrated the feasibility and processing advantages of contacting graphene using e-beam assisted Pt deposition. Using this deposition method, Pt can be directly deposited on CVD-grown graphene immediately following CVD growth, while graphene remains on the metal catalyst. Following deposition, the Pt/graphene can be successfully transferred to an insulating substrate using a typical wet-transfer technique. The deposition method leaves the graphene intact, and we observed an increase in the Raman D-mode in the graphene contacted by Pt, which may be due to localized heating during deposition, or hydrogen-induced graphene etching from remnants of cracked organometallic precursor gas. Such an increase in D-mode indicates the presence of dangling bonds in the graphene structure which should facilitate bonding to the metal and chemisorption of the Pt to the graphene. Using e-beam assisted Pt deposition in conjunction with masked CVD growth, we demonstrated that complete graphene devices may be fabricated with minimized graphene processing steps. This lays the groundwork for reducing common challenges as well as defects and damage to graphene that can routinely occur in photolithography, e-beam lithography, and shadow mask processing. We performed an order of magnitude estimate of the contact resistance and found the contact resistivity to be on the order of $10^9\ \Omega\ \mu m$. The reasons for high contact resistance ultimately do not undermine the utility and advantages of the processing techniques demonstrated herein, and we have laid the groundwork for future research in this field involving

Redistribution subject to AVS license or copyright; see http://scitation.aip.org/termsconditions. IP: 155.98.6.186 On: Tue, 02 Aug 2016 22:40:18

graphene device fabrication and processing via e-beam assisted metal deposition.

ACKNOWLEDGMENTS

The authors wish to thank Randy Polson for technical assistance in using the FEI Helios Nanolab 650 Dual Beam instrument, as well as the Department of Energy (Grant No. DE-FG02-04ER46148) for financial support.

[1]T. Yu, C. W. Liang, C. Kim, E. S. Song, and B. Yu, IEEE Electron Device Lett. **32**, 1110 (2011).
[2]T. Palacios, A. Hsu, and H. Wang, IEEE Commun. Mag. **48**, 122 (2010).
[3]S. Bae *et al.*, Nat. Nanotechnol. **5**, 574 (2010).
[4]W. Hu, C. Peng, W. Luo, M. Lv, X. Li, D. Li, Q. Huang, and C. Fan, ACS Nano **4**, 4317 (2010).
[5]E. K. Wujcik and C. N. Monty, Wiley Interdiscip. Rev. Nanomed. Nanobiotechnol. **5**, 233 (2013).
[6]S. Pisana, P. M. Braganca, E. E. Marinero, and B. A. Gurney, IEEE Trans. Magn. **46**, 1910 (2010).
[7]R. Sun, Y. Zhang, K. Li, C. Hui, K. He, X. Ma, and F. Liu, Appl. Phys. Lett. **103**, 013106 (2013).
[8]X. Li *et al.*, Science **324**, 1312 (2009).
[9]X. Liang *et al.*, ACS Nano **5**, 9144 (2011).
[10]X. Dong, D. Fu, W. Fang, Y. Shi, P. Chen, and L. J. Li, Small **5**, 1422 (2009).
[11]J. A. Robinson, M. Labella, M. Zhu, M. Hollander, R. Kasarda, Z. Hughes, K. Trumbull, R. Cavalero, and D. Snyder, Appl. Phys. Lett. **98**, 053103 (2011).
[12]R. Shi, H. Xu, B. Chen, Z. Zhang, and L. M. Peng, Appl. Phys. Lett. **102**, 113102 (2013).
[13]Y. Yang, L. I. Huang, Y. Fukuyama, F. H. Liu, M. A. Real, P. Barbara, C. Te Liang, D. B. Newell, and R. E. Elmquist, Small **11**, 90 (2015).
[14]W. Bao, G. Liu, Z. Zhao, H. Zhang, D. Yan, A. Deshpande, B. LeRoy, and C. N. Lau, Nano Res. **3**, 98 (2010).
[15]S. J. Randolph, J. D. Fowlkes, and P. D. Rack, Crit. Rev. Solid State Mater. Sci. **31**, 55 (2006).
[16]N. Silvis-Cividjian, C. W. Hagen, and P. Kruit, J. Appl. Phys. **98**, 084905 (2005).
[17]R. H. Siller, W. A. Oates, and R. B. McLellan, J. Less Common Mater. **16**, 71 (1968).
[18]J. D. Barry, M. Ervin, J. Molstad, A. Wickenden, T. Brintlinger, P. Hoffman, and J. Meingailis, J. Vac. Sci. Technol., B **24**, 3165 (2006).
[19]S. A. Boden, Z. Moktadir, D. M. Bagnall, H. Mizuta, and H. N. Rutt, Microelectron. Eng. **88**, 2452 (2011).
[20]N. S. Safron, M. Kim, P. Gopalan, and M. S. Arnold, Adv. Mater. **24**, 1041 (2012).
[21]K. R. Williams, K. Gupta, and M. Wasilik, J. Microelectromech. Syst. **12**, 761 (2003).
[22]D. M. Shirk and A. P. Molian, Carbon N. Y. **39**, 1183 (2001).
[23]M. G. Stanford, B. B. Lewis, J. H. Noh, J. D. Fowlkes, N. A. Roberts, H. Plank, and P. D. Rack, ACS Appl. Mater. Interfaces **6**, 21256 (2014).
[24]A. Botman, M. Hesselberth, and J. J. L. Mulders, Microelectron. Eng. **85**, 1139 (2008).
[25]C. Castiglioni, F. Negri, M. Rigolio, and G. Zerbi, J. Chem. Phys. **115**, 3769 (2001).
[26]P. A. Khomyakov, G. Giovannetti, P. C. Rusu, G. Brocks, J. Van Den Brink, and P. J. Kelly, Phys. Rev. B **79**, 195425 (2009).
[27]W. S. Leong, C. T. Nai, and J. T. L. Thong, Nano Lett. **14**, 3840 (2014).
[28]B. Sommer, J. Sonntag, A. Ganczarczyk, D. Braam, G. Prinz, A. Lorke, and M. Geller, Sci. Rep. **5**, 7781 (2015).
[29]K. Nagashio, T. Nishimura, K. Kita, and A. Toriumi, IEEE Int. Electron Devices Meet. **2009**, 1.
[30]J. T. Smith, A. D. Franklin, D. B. Farmer, and C. D. Dimitrakopoulos, ACS Nano **7**, 3661 (2013).
[31]I. Utke, P. Hoffmann, and J. Melngailis, J. Vac. Sci. Technol., B **26**, 1197 (2008).
[32]I. Vlassiouk, P. Fulvio, H. Meyer, N. Lavrik, S. Dai, P. Datskos, and S. Smirnov, Carbon N. Y. **54**, 58 (2013).
[33]G. Giovannetti, P. A. Khomyakov, G. Brocks, V. M. Karpan, J. Van Den Brink, and P. J. Kelly, Phys. Rev. Lett. **101**, 026803 (2008).
[34]J. S. Moon *et al.*, IEEE Electron Device Lett. **31**, 1193 (2010).
[35]S. Russo, M. F. Craciun, M. Yamamoto, A. F. Morpurgo, and S. Tarucha, Phys. E Low-Dimensional Syst. Nanostruct. **42**, 677 (2010).
[36]R. M. Langford, T. X. Wang, and D. Ozkaya, Microelectron. Eng. **84**, 784 (2007).
[37]A. Botman, J. J. L. Mulders, and C. W. Hagen, Nanotechnology **20**, 372001 (2009).
[38]J. C. Lascovich, R. Giorgi, and S. Scaglione, Appl. Surf. Sci. **47**, 17 (1991).
[39]P. K. Chu and L. Li, Mater. Chem. Phys. **96**, 253 (2006).
[40]See supplementary material at http://dx.doi.org/10.1116/1.4958795 for specific experimental details: parameters for CVD graphene growth, graphene transfer, Pt deposition, characterization and measurement techniques, and methods for Al_2O_3-masked graphene growth.

Redistribution subject to AVS license or copyright; see http://scitation.aip.org/termsconditions. IP: 155.98.6.186 On: Tue, 02 Aug 2016 22:40:18